HAL WATSON, JR.
Assistant Professor of Solid Mechanics

Southern Methodist University
Institute of Technology
Dallas, Texas 75222

ABSTRACT

Short specimens of Armco iron were tested at room temperature under compressive, axial loads at strains up to 0.6% and strain rates up to 10^3 in/in-sec. During loading, the axial stress was measured with a thin, piezoceramic disk inserted between the specimen and loading bar. The surface strain was measured with conventional epoxy-backed, foil strain gages, and the strain rate deduced by differentiating the strain vs. time record. The stress, strain, and strain rate data were plotted and were found to be approximated by a particular constitutive functional. The constitutive equation was then used along with the governing equations of motion and continuity in finding a numerical solution to the problem of a one-dimensional plastic wave propagating in a rate sensitive bar caused by an initial axial stress $\sigma(0,t)$. The solutions at two locations for both stress and strain were found to compare favorably with the stress and strain measured in a long bar impact test.

INTRODUCTION

It is generally accepted that most engineering materials are, to some degree, rate sensitive; that is, the materials exhibit the property in a dynamic test, of being able to support a greater stress, at a particular value of strain, than that observed, at the same strain, in a quasi-static test. It has been observed that some materials, such as the body-centered-cubic metals, are highly rate sensitive at low rates of straining, while others, such as the face-centered-cubic metals, are only slightly rate sensitive under the extremes of impact loading rates.[1,2,3,4] Both of these observations can be explained by the dislocation theory of plastic deformation, which attributes the strain rate effect to the obstruction of the progress of dislocations as they migrate through the material. Body-centered-cubic metals have been found to contain more dislocation locking mechanisms and to possess fewer mechanisms of slip, and therefore, to offer more obstruction to dislocations, than the face-centered cubics. It has been shown that macroscopic creep, stress-strain, and impact tests can all be interpreted in terms of a strain rate equation that is based on the microscopic behavior of dislocations.[5]

In order to determine the degree of rate sensitivity, or constitutive law, of a material, the stress and strain must be measured simultaneously at a single point over a wide range of constant strain rates. Even if such ideal measurements could be performed, it would be necessary to assume that the measurements at the point were representative of every point in the entire batch of material; that is, that the material is perfectly homogeneous. To compound the difficulties, any constitutive relationship inferred from the measurements is valid only for the particular environmental testing conditions of the tests. Changes in temperature and pressure can greatly affect the stress-strain relationship.[2,4,6]

The experimental technique used in this investigation has been used to measure the dynamic stress-strain characteristics of aluminum under normal conditions and of copper and iron at pressures up to 100 Ksi and at temperatures up to 1000°F. This method allows the measurement of all three important quantities - stress (load), strain, and strain rate at essentially the same material location.[3,4,6]

A detailed discussion of the experimental technique used in the dynamic tests follows in a succeeding section. Since the tests were destructive

and the strain rate varied in each test, several specimens had to be tested at each impact velocity. Altogether, ten tests were performed on short specimens of Armco iron at strain rates up to 10^3 in/in-sec. The stress, strain, and strain rate data obtained in the short specimen tests were then compared to the data obtained from a wave propagation test on a long bar of specimen material. During the long bar test, the stress and strain measurements at two locations were recorded. The stress record at the first location provided the boundary condition for the stress $\sigma(x,t)$ at $x = 0$ to be used in the numerical solution of the equations of a one-dimensional plastic wave propagating in a rate sensitive material. The stress-strain-strain rate relationship determined from data taken from the short specimen tests, and verified in long bar tests, provided the constitutive relation needed in the solution of the equations.

EQUATIONS

The equations used in the mathematical description of a one dimensional stress wave propagating in a rate sensitive material are those which were introduced by Sokolovsky.[7] One dimensional theory was applicable because of the magnitudes of strains, strain rates, and stress rates which were present in the tests. Higher rates would require the use of a two or three-dimensional theory with all of the complications of programming the equations not to mention those of determining which constitutive relations, what boundary conditions, and what yield conditions to assume.[8-11] Incorrect use of assumptions of these quantities are likely to cause greater errors in solution than a simpler theory.

The governing equations of motion and of continuity are:

$$\frac{\partial \sigma_x}{\partial x} = \rho \frac{\partial v}{\partial t} \tag{1}$$

$$\frac{\partial v}{\partial x} = \frac{\partial \varepsilon}{\partial t} \tag{2}$$

where x is the Lagrangian coordinate of a material point originally a distance x from the loaded end, σ_x is the axial stress, ρ is the original mass density, v is the particle velocity and ε is the strain. The strain is assumed to be comprised of two parts - the elastic part ε_E and the plastic

part ε_p - such that

$$\varepsilon = \varepsilon_E + \varepsilon_p \quad ;$$

therefore,

$$\frac{\partial \varepsilon}{\partial t} = \frac{\partial \varepsilon_E}{\partial t} + \frac{\partial \varepsilon_p}{\partial t} \quad . \tag{3}$$

It is assumed that

$$\frac{\partial \varepsilon_E}{\partial t} = \frac{1}{E} \frac{\partial \sigma}{\partial t} \tag{4}$$

in which E is Young's modulus, and

$$\frac{\partial \varepsilon_p}{\partial t} = g(\sigma,\varepsilon). \tag{5}$$

The latter is the so called "g" function which must be determined from experimental data. Eq. (3)-(5) can be combined to form

$$\frac{\partial \varepsilon}{\partial t} = \frac{1}{E} \frac{\partial \sigma}{\partial t} + g(\sigma,\varepsilon) \quad , \tag{6}$$

which is the constitutive equation. Equations (1), (2), and (6) form a hyperbolic set of first order partial differential equations which can be solved by means of the method of characteristics.[12] After applying the method of characteristics, a new set of characteristic differential equations emerge which are valid along certain characteristic directions. These are:

Characteristic Equation	Differential Equation for Characteristic Curves
$d\sigma - \rho C_o dv = -g(\sigma,\varepsilon)$	$dx = C_o dt$
$d\sigma + \rho C_o dv = -g(\sigma,\varepsilon)$	$dx = -C_o dt$
$d\sigma - E d\varepsilon = -g(\sigma,\varepsilon)$	$dx = 0$

where $C_o = (E/\rho)^{1/2}$. The characteristic equations are usually nonlinear because of the nonlinear character of $g(\sigma,\varepsilon)$. Although few closed form solutions are attainable for these equations, they are easily programmed for a digital computer after the usual finite difference approximations for

the derivatives have been made. The ease of programming is due to the fact that the characteristic curves are straight lines in the x-t plane (Fig. 1). The only difficulties which arise are due to the fact that finite differencing the characteristic equations yields a set of three nonlinear algebraic equations to be solved at each point x,t for σ,ε, and v. The problem is thus reduced to solving for the roots of a set of three nonlinear algebraic equations at every point. In the program, a scheme employing a predictor-corrector, iterative procedure is followed until predicted set of values of σ,ε, v agree with a previously predicted set to a certain preset number of digits. There is no problem of computation along the line x = 0 since the stress is defined on that boundary. However, along the line $x = C_o t$ the following jump conditions must be employed.

$$\Delta\sigma = -\rho C_o \Delta v$$
$$\Delta v = -C_o \Delta\varepsilon \qquad (8)$$

where Δ denotes a jump in value of σ, ε, and v after arrival of the elastic wave front. These two jump conditions result from equating impulse to change of momentum for the traversing of an element of the bar by the shock wave and from a consequence of the continuity of displacement across the shock, respectively. These conditions allow the computation of σ, ε, and v along the elastic wave front so that points in the interior of the mesh in the x-t plane can be determined.[6,12]

The initial conditions are

$$\sigma(x,0) = v(x,0) = \varepsilon(x,0) = 0 \qquad x > 0$$

and the boundary condition is

$$\sigma(0,t) = f(t) \qquad t \geq 0$$

which is a function which approximates the stress vs. time record at the first location of a long bar test.

THE EXPERIMENTAL METHOD

The experimental method used in the dynamic testing is a variation of the split hopkinson pressure bar technique. However, this variation of the technique does not require the critical assumption of uniformity of stress, strain, and strain rate over the entire length of the specimen, an assump-

tion which is necessary in reducing the raw data taken from a split hopkinson bar experiment.

This variation of the split hopkinson bar technique includes the use of a thin, calibrated, piezoceramic(X-cut quartz) crystal, which is sandwiched between a hardened steel loading bar and the softer specimen, in measuring the average stress over the cross section of the specimen (Fig. 2). On the surface of the specimen, very near the quartz crystal, is mounted an electrical resistance strain gage for measuring the axial strain. The slope of the strain vs. time record provided the strain rate. It can be assumed that the stress, strain, and strain rate are being measured at essentially the same material point, if the following assumptions can be used in the reduction of data from this type of test: (1) the stress is uniform and axial over the cross section, (2) the difference between the stress at the crystal and the stress on the cross section beneath the strain gage is insignificant, (3) the surface strain is representative of the axial strain at every point on the cross section beneath the gage, and (4) lateral inertia effects on the axial stress are negligible. Arguments in support of each of these assumptions have been made elsewhere but will be outlined in the following paragraphs.[3,4]

On a typical dynamic test on a short, metal specimen, a flat-nosed hardened steel projectile is propelled along the evacuated barrel of a light gas gun and is allowed to impact the longer, hardened steel loading bar, one end of which is positioned inside the gun barrel near the muzzel. The impact gives rise to an elastic stress wave, which propagates along the loading bar, through the quartz crystal, and into the specimen. As the stress pulse passes through the quartz crystal into the specimen, a stress exceeding the static yield stress of the material is impressed on the front face of the test specimen, forcing it to be strained into the plastic range. During the plastic deformation, the value of the average stress over the cross section of the specimen is measured by means of the quartz disk which generates an electrical charge proportional to the average stress over the cross section. The charge is then collected on a capacitor and the voltage across the capacitor is measured. Chalupnik[4] has shown that the effect on the stress wave due to the presence of the thin quartz disk is almost negligible, the only effect being a small increase in the rise time of the transmitted pulse of about one microsecond for a steel-quartz-iron configuration. The quartz

crystal-capacitor system is calibrated for stress by replacing the specimen with a calibrated hardened steel load cell having the same dimensions, and allowing an elastic wave to propagate through the load cell. The surface strain on the load cell together with its calibration curve (Young's modulus) are then used to calibrate the quartz disk. A calibration test record is shown in Fig. 3. The system calibration was found to be 26,500 psi/volt.

Very near the quartz crystal (1/8 in. for 0.50 in. diam. specimen) a foil, resistance strain gage is attached in order to measure the axial surface strain near the disk. The measured values of surface strain at this location is assumed to be representative of the average axial strain over the material cross section beneath the strain gage. This assumption is reasonable from material continuity considerations if after the test, the faces of the extreme ends of the specimen are found to be parallel and no local barreling is evident along the length of the specimen. Although the strain gage and the load transducer are not at the exact same location along the length of the specimen, it can be shown that only in regions of very large time derivatives of stress $\partial\sigma/\partial t$ and of very large strains, such regions as are found near the impact end of a soft specimen undergoing direct, high velocity projectile impact does the small difference in spatial location give rise to appreciable error. For dynamic testing of this type in which the stress wave has traveled along a long loading bar and has undergone the subsequent dispersion of its high frequency components, it can be shown, as well as observed, that the stress rates are not of sufficient magnitude to cause large spatial errors except very near the wave front. Since we measure stress vs. time, it is a simple matter to limit the gathering of stress-strain data to regions of negligible stress rate.[4,6]

Errors due to antisymmetric loading were minimized by careful alignment of the loading bar projectile and loading bar specimen interfaces and by use of machine-lapped interfaces. A number of dynamic tests were performed to check the accuracy of alignment and symmetry of loading by separately measuring the strain on diametrically opposed positions at a particular material cross section. The stress vs. time record also provides a check on the alignment during each test. It has been found by the author that an antisymmetric loading causes a dramatic change in the shape of the stress vs. time record; in particular the rise time is greatly increased. The author found that a

rise time of five microseconds or less in a test of this type is a good indication of symmetric loading.

The question always arises in tests of this type as to whether or not the assumptions of one-dimensional stress and of negligible radial inertia effects on the axial stress are valid. In view of the type of loading and geometry (the wave length of the axial stress pulse is greater than the diameter of the specimen) the first assumption seems quite reasonable; however, radial inertia effects due to radial accelerations caused by radial straining are expected to be significant beyond a certain loading rate. Moreover as Devault[13] has shown it is inherently quite difficult to separate strain rate effects from radial inertia effects. Hunter and Davies[14] have shown that significant radial inertia effects are to be expected in regions where the time derivative of strain rate is large. The author has observed from the stress and strain records that in tests of this kind, the regions of large time derivatives of strain rate occur at times of large stress rate, regions in which one must reject the data in order that $\partial\sigma/\partial x$ be negligible. Therefore, the author assumes radial inertia effects to be negligible in the regions in which $\dot{\sigma} \approx 0$ where the raw data was gathered. Additional tests have supported this assumption. In these tests, copper and iron were tested by the experimental method described herein at elevated temperatures.[6] It was found that the rate sensitivity of copper increased with temperature and the rate sensitivity of iron remained almost unchanged over the test range of temperatures. It was expected that radial inertia effects, not being greatly dependent on stress-strain properties, would remain fairly constant over the temperature range for both materials, although the same was not expected for the stress-strain characteristics themselves. No such constancy was revealed in the data reduction; the stress strain properties of each material changed independently of the other, as expected.

SPECIMEN PREPARATION

A chemical analysis of random samples of the specimen material, Armco iron, was obtained and revealed the following impurities:

0.02%	carbon
0.012%	sulfur
0.008%	phosphorous

The specimen material was furnished by the manufacturer in 3/4 inch rounds. The rounds were turned down to 1/2 inch rounds, cut off in 1 inch lengths, and faced off in a lathe. The 1 inch lengths were then annealed in an evacuated furnace at 1500°F for one hour and allowed to furnace cool. Each specimen was then lapped flat on each end and prepared for the attachment of strain gages. Two 1/8 inch gage lengths epoxy-backed strain gages were attached, diametrically opposed, onto each specimen 1/16 inch from the end with a heat curing epoxy. A tiny drop of epoxy allowed the quartz crystal to be attached to the specimen. Then the specimen was soaked in a 200°F oven for two hours.

TEST RESULTS AND DATA REDUCTION

The outputs of the stress and strain circuits were connected to a dual-beam, 10 MHz oscilloscope and the oscillograms recorded on Polaroid film. The oscilloscope was triggered by the output voltage of a small piezoelectric accelerometer attached to the surface of the loading bar which responds to the passage of the stress wave. In this way the oscilloscope was synchronized to the event of the stress wave entering the quartz crystal. A typical stress and strain vs. time record taken from the Polaroid photograph and enlarged is shown in Fig. 4. One observes from the figure that during the passage of the wave front the stress rate and rate of change of strain rate are quite large ($\dot{\sigma} \approx 10^{10}$ psi/sec, $\ddot{\varepsilon} \approx 3 \times 10^{7}$ in/in-sec^2); however, about 10^{-5} sec <u>after</u> the passage of the wave front both $\dot{\sigma}$ and $\ddot{\varepsilon}$ are very nearly zero. It is in this region that radial inertia effects and stress gradients are small and where the data for this investigation was taken. The values for the two data points in Fig. 4 are:

$$\dot{\sigma} \simeq \ddot{\varepsilon} \simeq 0, \quad \sigma = 65{,}200 \text{ psi}, \quad \varepsilon = 0.5\%, \text{ and } \dot{\varepsilon} = 300 \text{ in/in-sec.}$$

The data from the short specimen tests are plotted in Fig. 5 in which stress is plotted vs. strain for several strain rates. Also shown on the figure is the quasi-static curve taken from a test in which a hydraulic testing machine was used. The data points for the σ vs. ε at $\dot{\varepsilon} = 1$ in/in-sec. were obtained similarly. One can infer from the data that iron is certainly rate sensitive in this range of strains and strain rates. If such data are to be useful in predicting the progress of a plastic wave in a long bar, they must be expressed in some functional form. Several investigators have proposed particular functionals in describing the rate sensi-

tivity of certain materials. Some of these are listed below in which the rate sensitivity is expressed by the "g" function (Note: $\dot{\varepsilon} = g(\sigma,\varepsilon)$ for $\dot{\sigma} = 0$ from Eq. 6)

$g(\sigma,\varepsilon)$	Domain	Investigator
$K(\sigma - \sigma_y)$	$\sigma > \sigma$	Sokolovsky[7]
$K(\sigma - \bar{\sigma})$	$\sigma > \bar{\sigma}$	Malvern[15]
$K(\sigma/\bar{\sigma})^n$	$\sigma > \bar{\sigma}$	Chiddister[2]
$K\left[\frac{\sigma-\bar{\sigma}}{\bar{\sigma}}\right]^n$	$\sigma > \bar{\sigma}$	Chalupnik[4]
0	$\sigma \leq \bar{\sigma}$	All of the above

in which $\bar{\sigma}$ is the value of stress at strain ε in a quasi-static test, σ_y is the static yield stress, and both K and n are material parameters which depend only on environmental conditions such as ambient temperature or pressure. In describing the data, one attempts to determine values for the parameters, K and n, which permit the functional form to provide the best fit to the data. Several functional forms were tried in an attempt to describe the data shown in Fig. 5. The form which proved to provide the best fit is the one shown in Eq. 9 proposed by Chalupnik.[4] The functional is of such a form that if $\log_{10}\left[\frac{\sigma-\bar{\sigma}}{\bar{\sigma}}\right]$ is plotted vs. $\log_{10}\dot{\varepsilon}$ the data points lie on a straight line, the slope of which yields n and the intercept of which yields K. The data from Fig. 5 were plotted on such a log plot (Fig. 6). As shown, the data points do not lie along a straight line; however, they do lie inside a linear band. Thus this functional form could be used as a first approximation to the constitutive equation for the material. If the dashed line inside the linear band is used as the line along which the data points are assumed to lie, the values for K and n can be calculated. These values are $K = 50\ \text{sec}^{-1}$ and $n = 5.2$. The values for K for the upper and lower lines forming the linear band are $K = 25\ \text{sec}^{-1}$ (upper) and $K = 100\ \text{sec}^{-1}$ (lower).

LONG BAR TESTS

In a long bar test, the hardened steel back bar is replaced by a long bar of specimen material to which a quartz crystal and strain gages are attached. Thus the specimen and back bar of specimen material form essentially a long bar of specimen material with an embedded quartz crystal (Fig. 2b). During an impact test the quartz crystals supply the average stress vs. time information at the two cross sections and the strain gages supply the strain information at essentially the same locations. Any effect of the embedded quartz crystal on the stress wave has been found to be negligible provided the specimen and back bar are properly aligned and the interfaces properly lapped so that there are no gaps to cause reflections.[2,3] The stress wave will pass through the quartz crystal with only a slight increase in rise time. If any reflections of the wave occur, they are immediately noticeable in the stress record of the embedded quartz disk.

The results of a typical long bar test on iron is shown in Fig. 7 for the two strain vs. time records and in Fig. 8 for the two stress vs. time records. Each strain record shows a region of high strain rate at the elastic wave front followed by a region of lower strain rate in plastic range. The stress records show a very short rise time (5 microseconds), a region of high stress rate, at the wave front followed by a region of low stress rate. A quantitative comparison of the long bar stress, strain, and strain rate data is consistent with the data taken from short specimen tests.

NUMERICAL SOLUTION

The computer program, written for the solution of the nonlinear algebraic equations which resulted from the finite differencing of Eq. 9, included a variable mesh size scheme.[16,17] At $t = 0$, and for short times thereafter, the derivatives of all three variables are quite large. To minimize discretization error the program started with a $\Delta t = 10^{-10}$ sec or $\Delta x = 2 \times 10^{-5}$ in.; later in time these sizes were changed to $\Delta t = 5 \times 10^{-7}$ sec or $\Delta x = 1 \times 10^{-1}$ in. when the time derivatives were greatly reduced in magnitude.

The "g" function obtained from the short specimen tests was inserted into the program along with numerical values for Young's modulus and the density of iron. The boundary conditions for $\sigma(0,t)$ for $t \geq 0$ used in the program was taken from the stress record at $x = 0$ from a long bar test. In Fig. 8a the dashed curve, which is an approximation to the experimental stress record, is used as the boundary condition. This approximation was used instead of a least squares curve fit to the stress record because of programming difficulties. The programming was greatly simplified by assuming the stress boundary condition to be a step function followed by a polynomial function of time.

The program was written for a CDC 6600 digital computer in FORTRAN IV. Hand computations for solution of such problems are not practical because of the large number of computations. For example, computing out to 10^{-4} sec in propagation time requires computations at 5000 mesh points with approximately 15 iterations per mesh point and 60 mathematical operations per iteration - 5×10^6 operations.

The numerical solutions for strain and stress for three values of K are shown superposed on their experimental counterparts in Fig. 7 and 8 respectively. The general overall agreement between experiment and theory is quite good for $K = 50$ sec^{-1} and $n = 5.2$ up to 0.8% strain. All four strain curves at the second location reveal the large strain at the elastic front, more than twice the static yield strain, and the concave upward curvature immediately behind the wave front. Better agreement could be expected from a better functional representation of $\sigma(0,t)$; however, the constitutive law is only an approximation to the data itself, the values of K and n being computed from the dashed line (Fig. 5), for experimental data only up to 0.6% strain. Better agreement might be attained for $\varepsilon > 0.7\%$ by allowing K and n to be functions of ε and extending the range of strain in the short specimen tests beyond 0.6% strain.

CONCLUSIONS

It can be concluded from the tests and numerical solutions that iron is a highly strain rate sensitive material and that the strain rate sensitivity within the ranges of strain, strain rate, and stress rate to

which this study was limited, can be described by the function

$$\varepsilon = \frac{\dot{\sigma}}{E} + K\left[\frac{\sigma-\bar{\sigma}}{\bar{\sigma}}\right]^n$$

where $E = 28 \times 10^6$ psi

$K = 50\ \text{sec}^{-1}$

$n = 5.2$

Furthermore, the function obtained from short specimen test data can be shown to be consistent with long bar tests on the same material and can be used in a numerical solution of one dimensional equations of motion and continuity to predict, with reasonable agreement, the propagation of a plastic wave along the long bar of specimen material.

ACKNOWLEDGEMENTS

The author wishes to express his appreciation to Professor E. A. Ripperger of the University of Texas for his guidance during the experimental undertakings. The author is grateful for the financial support of this work at different times by the Army Research Office Contract DA-31-124-ARO-D-229, by the National Science Foundation Grant No. GK-3493, and by the Office of Naval Research Contract No. N00014-68-A-0515.

BIBLIOGRAPHY

1. Nadai, A. and Manjoine, M. J., "High Speed Tension Tests at Elevated Temperatures - Parts II and III," Journal of Applied Mechanics, Vol. 8, 1941, pp. A77-A91.

2. Chiddister, J. L. and Malvern, L. E., "Compression Impact Testing of Aluminum at Elevated Temperatures," Experimental Mechanics, Vol. 3, No. 4, pp. 81-90.

3. Karnes, C. H. and Ripperger, E. A., "Strain Rate Effects in Cold Worked High-Purity Aluminum," Journal of the Mechanics and Physics of Solids, Vol. 14, 1966, pp. 75-88.

4. Chalupnik, J. D. and Ripperger, E. A., "Dynamic Deformation of Metals under High Hydrostatic Pressure," Experimental Mechanics, Vol. 6, No. 11, pp. 547-554.

5. Gilman, J. J., "Progress in the Microdynamical Theory of Plasticity," Proceedings of the Fifth U.S. National Congress of Applied Mechanics, ASME, New York, 1966, pp. 385-405.

6. Watson. H., Jr., "The Effects of Strain-Rate and Temperature on the Stress-Strain Characteristics of Copper and Iron," unpublished Ph.D Thesis, The University of Texas, 1967.

7. Sokolovsky, V. V., "The Propagation of Elastic-Visco-Plastic Waves in Bars," Prikladia Matematika i Mekanika, Vol. 12, 1948, pp. 261-280.

8. Cooper, G. J. and Craggs, J. W., "Propagation of Elastic Waves," Journal of the Australian Mathematical Society, Vol. 6, 1966, pp. 55-64.

9. Cooper, G. J. and Craggs, J. W., "The Propagation of Plane Waves in Plastic Solids," Journal of the Australian Mathematical Society, Vol. 5, 1965, pp. 349-364.

10. Tapley, B. D. and Plass, H. J. Jr., "The Propagation of Plastic Waves in a Semi-Infinite Cylinder of a Strain-Rate Dependent Material," Proceedings of the Fifth Midwestern Conference on Solid Mechanics, 1961.

11. Karnes, C. H., Thorne, B. J., and Hermann, W., "Two Dimensional Elastic Plastic Behavior of a Rod Subjected to Axial Impact," Proceedings of the Fifth U. S. National Congress of Applied Mechanics, ASME, 1966, p. 568.

12. Malvern, L. E., "Plastic Wave Propagation in a Bar of Material Exhibiting a Strain Rate Effect," Quarterly of Applied Mathematics, Vol. 8, No. 4, 1951, pp. 405-411.

13. Devault, G. P., "The Effect of Lateral Inertia on the Propagation of Plastic Strain in a Cylindrical Rod,"Journal of the Mechanics and Physics of Solids, Vol. 13, 1965, pp. 55-68.

14. Hunter, S. C. and Davies, E. D. H., "The Dynamic Compression Testing of Solids by the Methods of the Split Hopkinson Pressure Bar - Part I - The Theoretical Mechanics of the Experiment," Armament Research and Development Establishment Report No. MX 8/60, Fort Halstead, Kent, England, 1960.

15. Malvern, L. E., "The Propagation of Longitudinal Waves of Plastic Deformation in a Bar of Material Exhibiting a Strain Rate Effect," Journal of Applied Mechanics, Vol. 18, 1951, pp. 203-208.

16. Ripperger, E. A. and Watson, Hal, Jr., "Strain-Rate Effects and Plastic Wave Propagation in Aluminum Rods," Proceedings of the Fifth U. S. National Congress of Applied Mechanics, ASME, 1966.

17. Ripperger, E. A. and Watson, Hal, Jr., "The Relationship between the Constitutive Equations and One-Dimensional Wave Propagation," Mechanical Behavior of Materials under Dynamic Loads, U. S. Lindholm, Editor, Springer-Verlag, New York, 1968.

FIGURE CAPTION LIST

Fig. 1 - Characteristic plane - after non-dimensionalizing all variable the characteristic lines $x = 0$, $x = C_o t$, and $x = -C_o t$ become $X = 0$, $X = T$, and $X = -T$. X and T are non-dimensional variables

Fig. 2 - (a) Schematic of the apparatus for a short specimen test; (b) Schematic of the changes in the set-up for a long bar test.

Fig. 3 - Quartz crystal calibration record.

Fig. 4 - Typical records of stress and strain vs. time from a dynamic test on a short specimen.

Fig. 5 - Stress vs. strain for several strain rates. Armco iron at room temperature.

Fig. 6 - Log-log plot of overstress ratio vs. strain rate for Armco iron at room temperature.

Fig. 7 - Typical long bar test data - strain vs. time at two locations. Superposed on test data are three numerical solutions for three different values of K.

Fig. 8 - Typical long bar test data - stress vs. time at two locations. Superposed on test data are three numerical solutions for three different values of K.

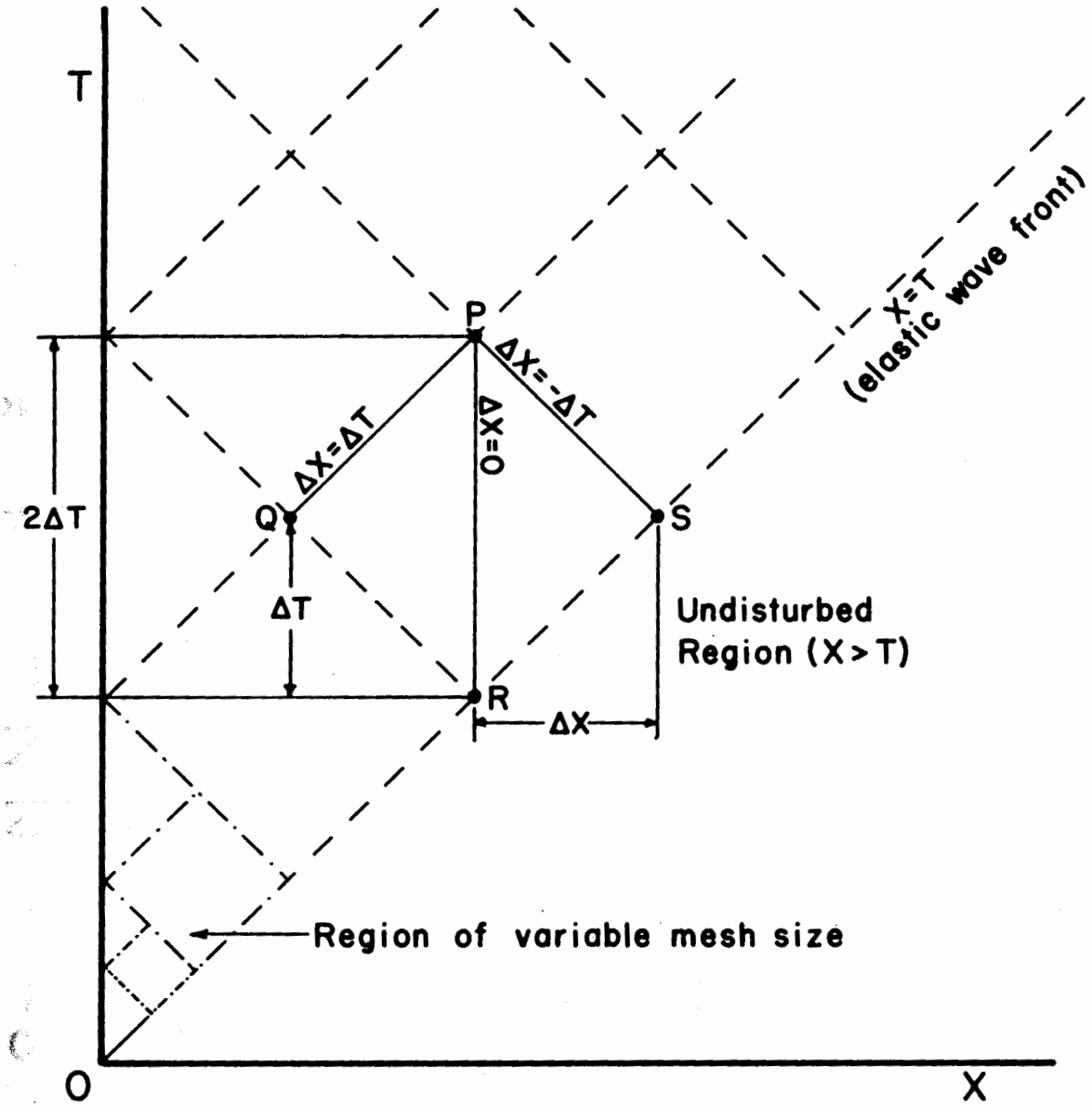
T
P
ΔX=-ΔT
X=T
(elastic wave front)
ΔX=ΔT
ΔX=0
2ΔT
Q
S
ΔT
Undisturbed
Region (X>T)
R
ΔX
Region of variable mesh size
O
X

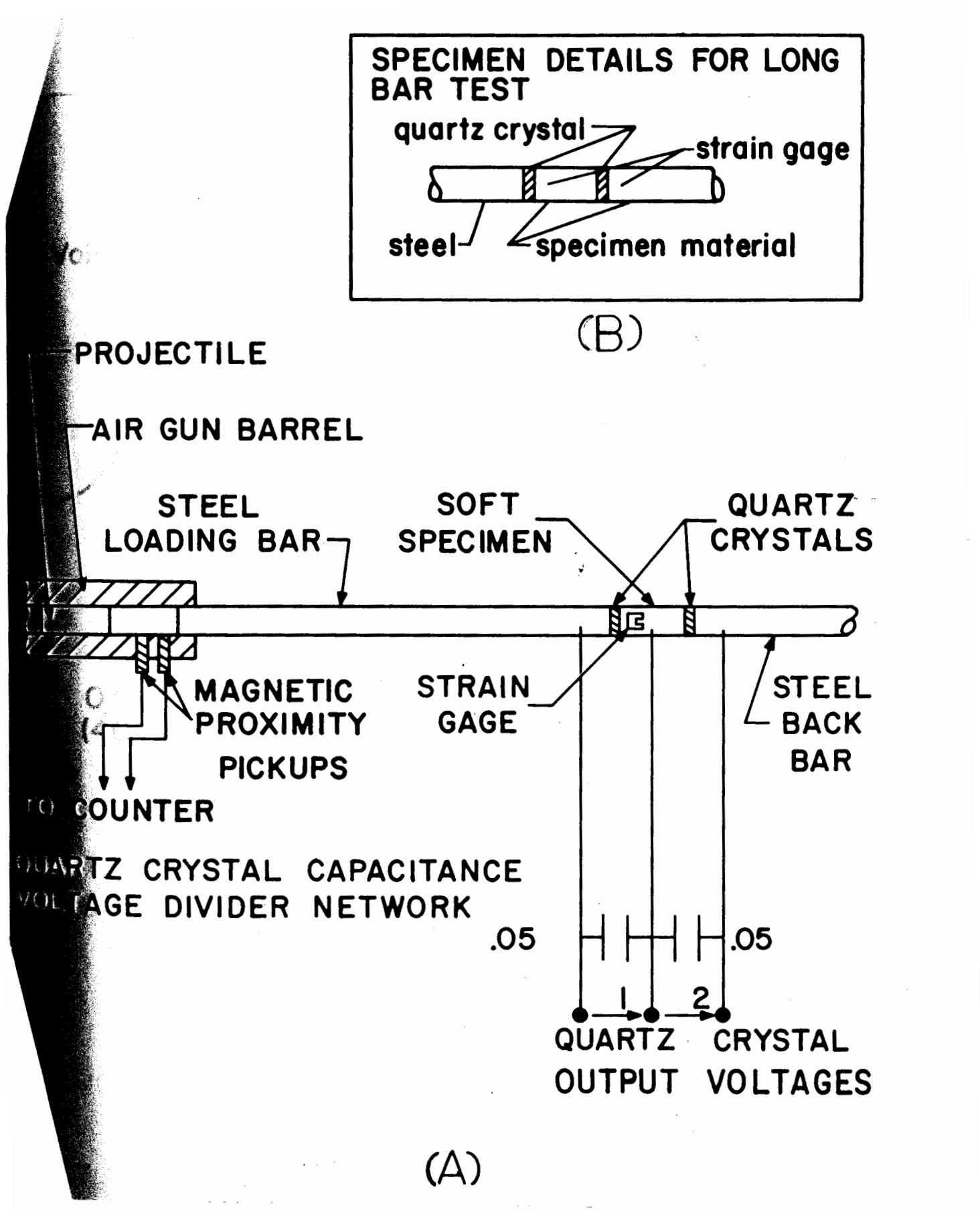
SPECIMEN DETAILS FOR LONG BAR TEST
quartz crystal
strain gage
steel
specimen material
(B)
PROJECTILE
AIR GUN BARREL
STEEL LOADING BAR
SOFT SPECIMEN
QUARTZ CRYSTALS
MAGNETIC PROXIMITY PICKUPS
STRAIN GAGE
STEEL BACK BAR
TO COUNTER
QUARTZ CRYSTAL CAPACITANCE VOLTAGE DIVIDER NETWORK
.05
.05
1
2
QUARTZ CRYSTAL OUTPUT VOLTAGES
(A)

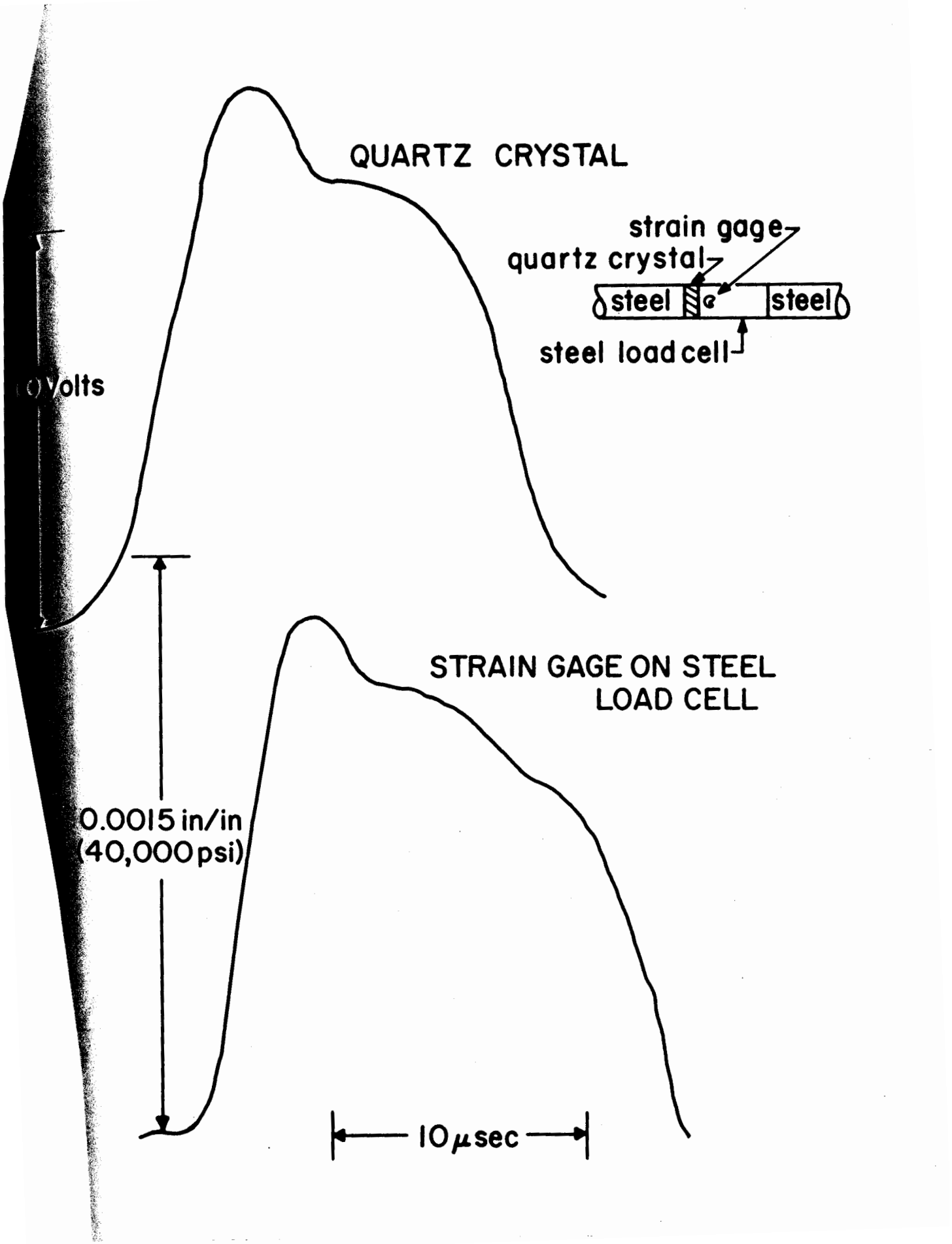
QUARTZ CRYSTAL
strain gage
quartz crystal
steel
steel
steel load cell
Volts
STRAIN GAGE ON STEEL
LOAD CELL
0.0015 in/in
(40,000 psi)
10 μsec

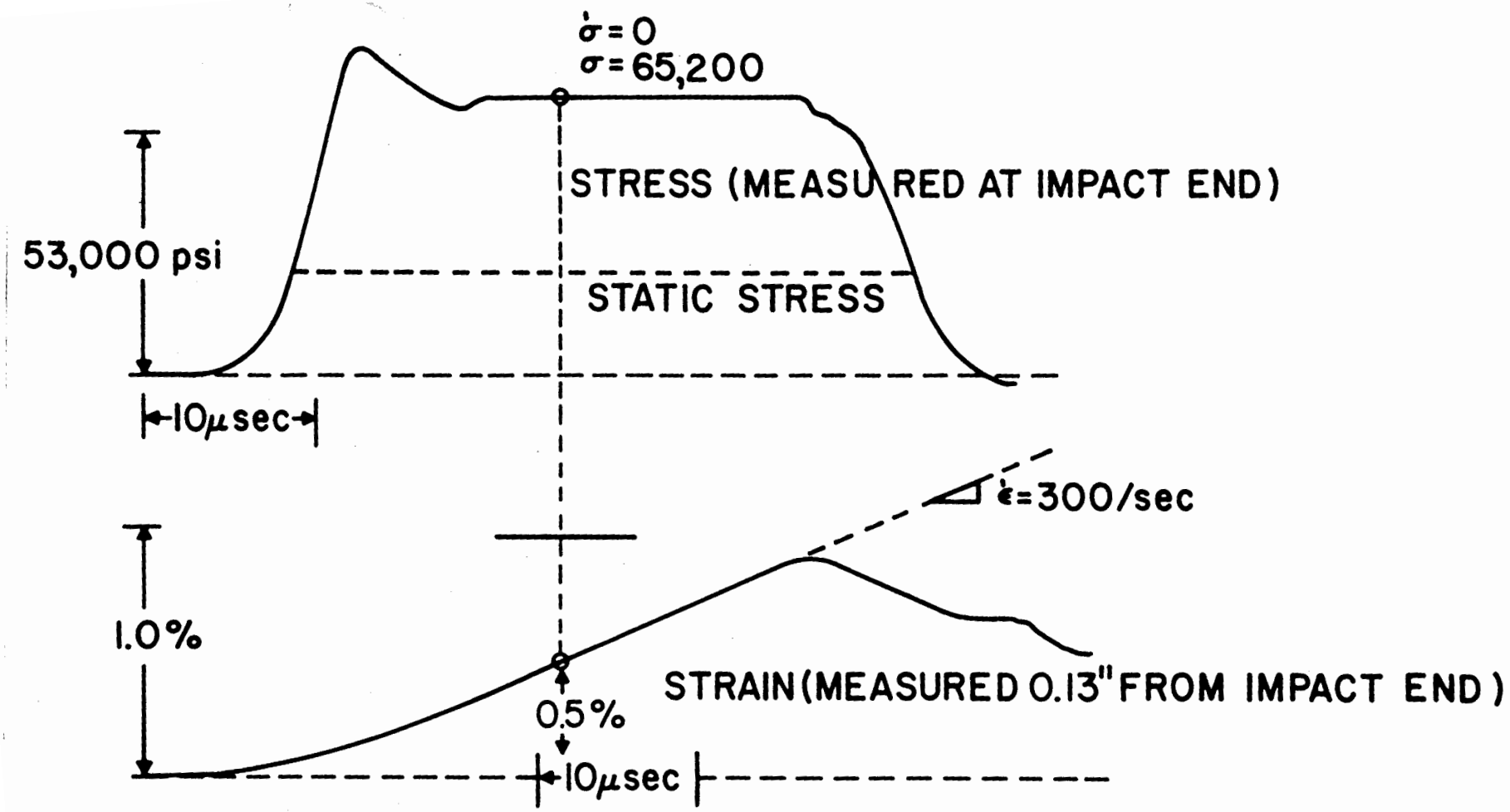
$\dot{\sigma}=0$
$\sigma=65{,}200$
STRESS (MEASURED AT IMPACT END)
53,000 psi
STATIC STRESS
10μsec
$\dot{\epsilon}=300/sec$
1.0%
STRAIN (MEASURED 0.13" FROM IMPACT END)
0.5%
10μsec

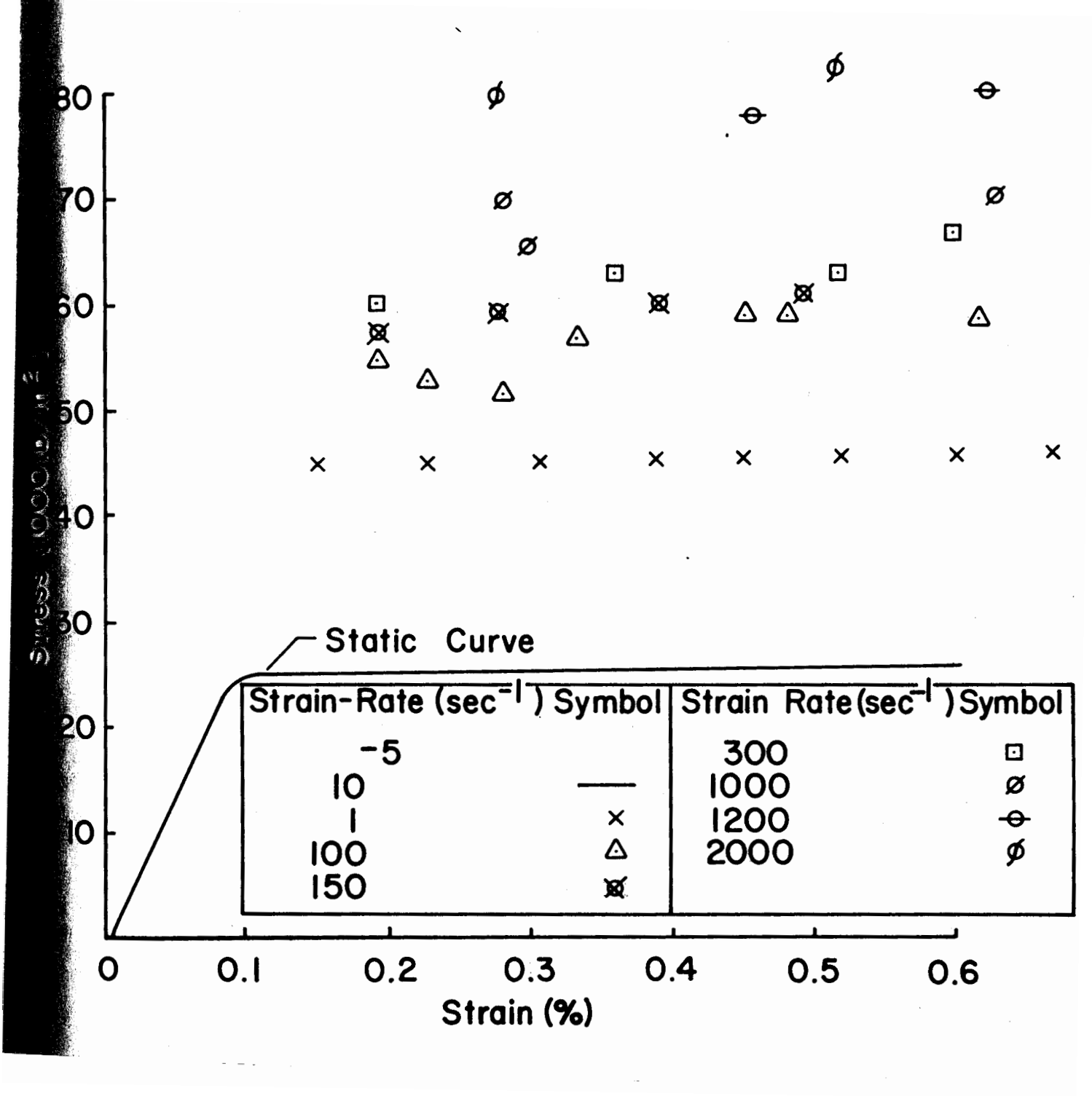
Stress (1000 lb/in²)
80
70
60
50
40
30
20
10
0
0.1
0.2
0.3
0.4
0.5
0.6
Strain (%)
Static Curve
Strain-Rate (sec⁻¹) Symbol
-5
10
1
100
150
Strain Rate (sec⁻¹) Symbol
300
1000
1200
2000

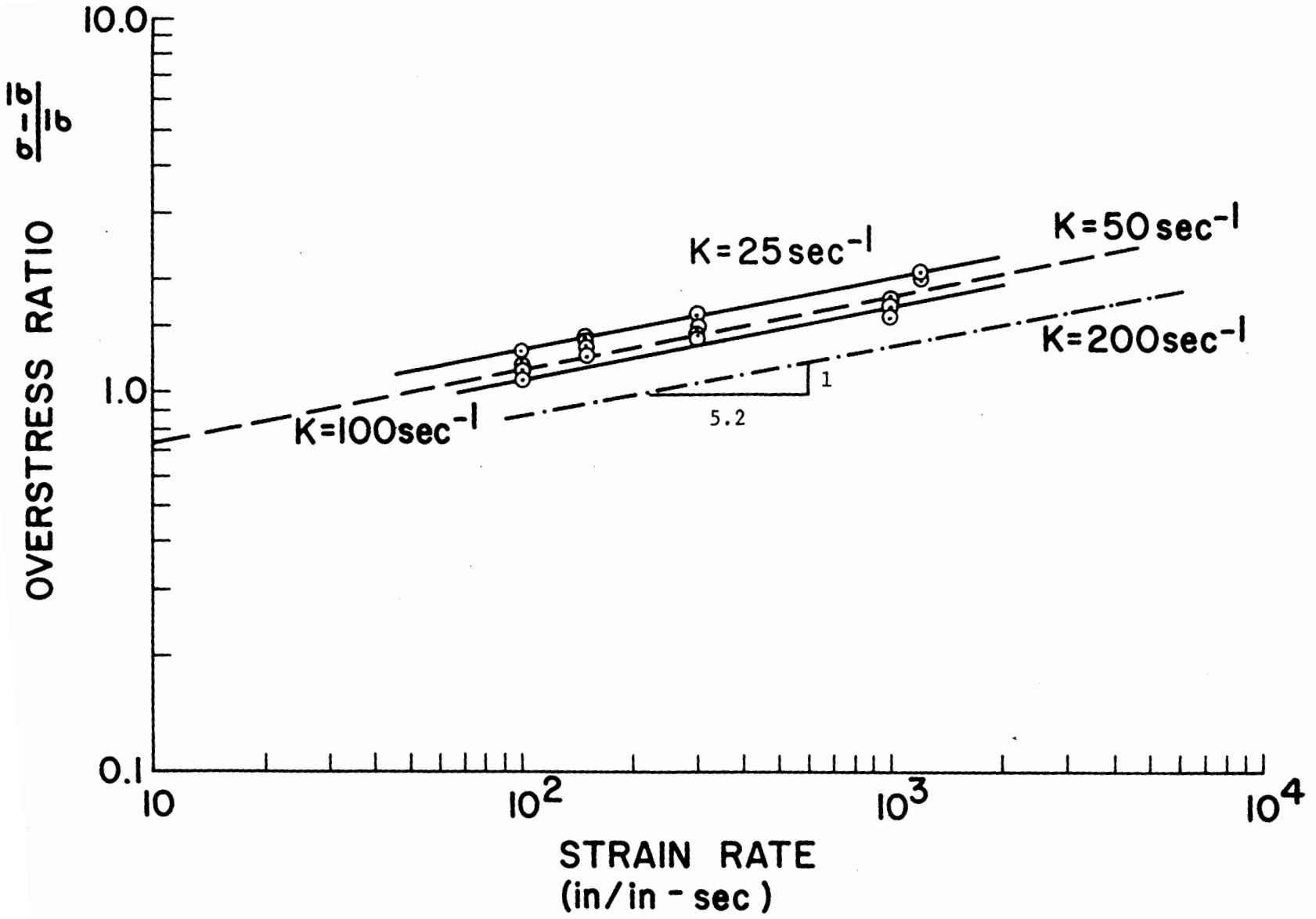
10.0
1.0
0.1
OVERSTRESS RATIO $\frac{\sigma-\bar{\sigma}}{\bar{\sigma}}$
K=25 sec^{-1}
K=50 sec^{-1}
K=100 sec^{-1}
K=200 sec^{-1}
1
5.2
10
10^2
10^3
10^4
STRAIN RATE
(in/in - sec)

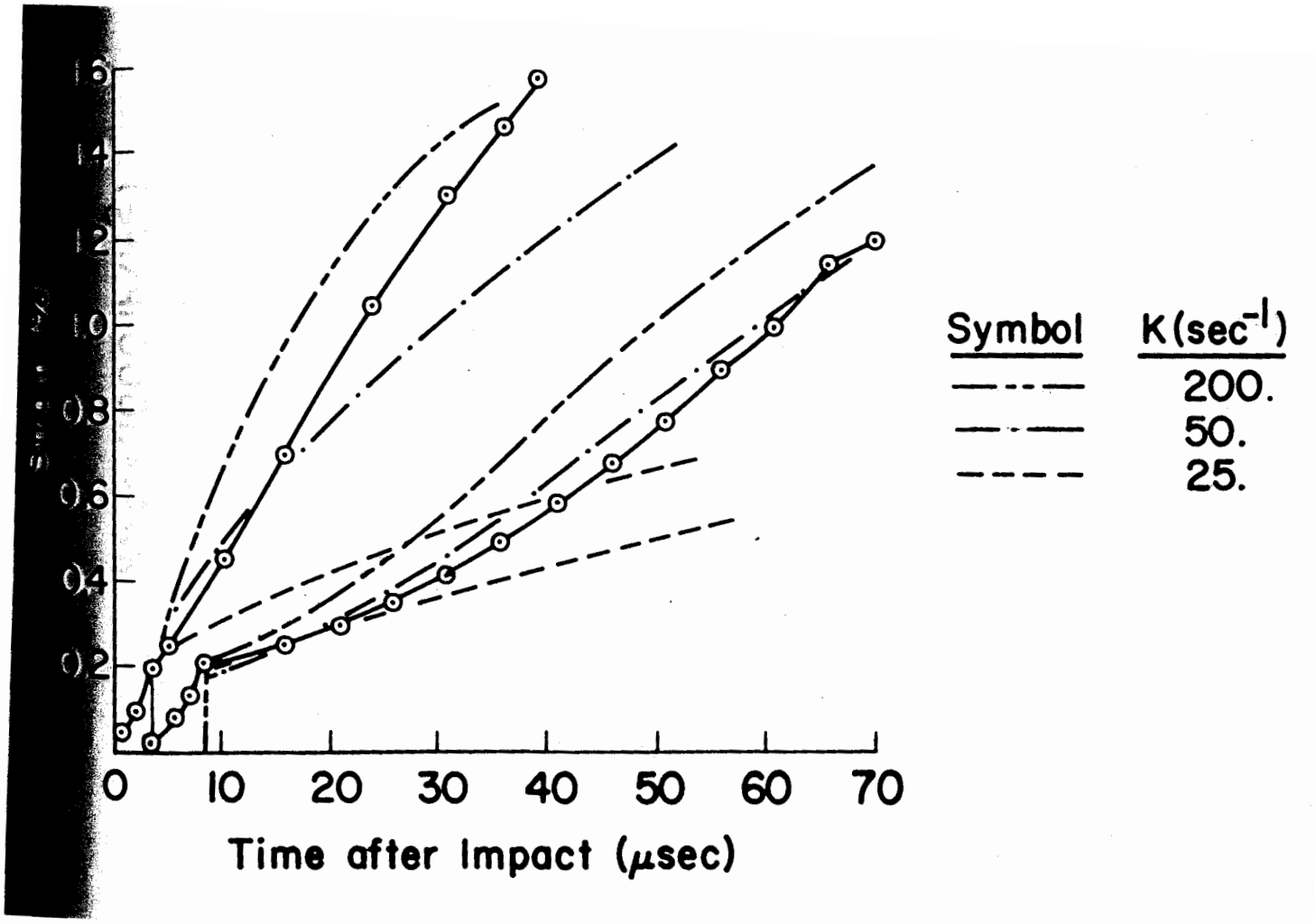
Symbol
K(sec⁻¹)
200.
50.
25.
0
10
20
30
40
50
60
70
Time after Impact (μsec)

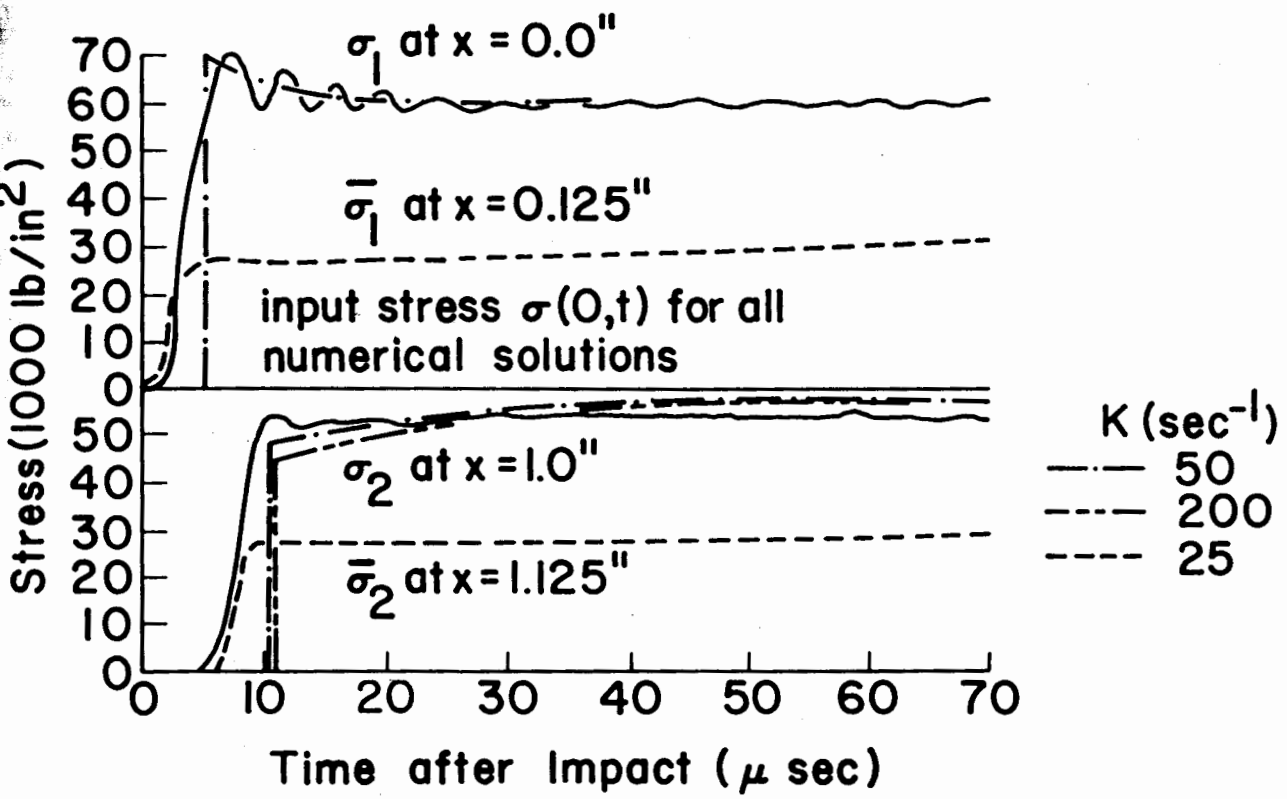
σ_1 at x = 0.0"
$\bar{\sigma}_1$ at x = 0.125"
input stress $\sigma(0,t)$ for all numerical solutions
σ_2 at x = 1.0"
$\bar{\sigma}_2$ at x = 1.125"
Stress (1000 lb/in^2)
Time after Impact (μ sec)
K (sec^{-1})
50
200
25